Applied Mathematics and Computation 457 (2023) 128164

Contents lists available at ScienceDirect

Applied Mathematics and Computation

journal homepage: www.elsevier.com/locate/amc

A 2D prediction step using multiquadric local interpolation with adaptive parameter estimation for image compression☆

Francesc Aràndiga[a], Rosa Donat[a,*], Daniela Schenone[b]

[a] Departament de Matemàtiques, Universitat de València (EG) (Spain)
[b] Konecranes Oyj

ARTICLE INFO

Keywords:
Weighted essentially non-oscillatory method
Radial basis function interpolation

ABSTRACT

We present and analyze several prediction strategies in the 2D setting based on multiquadric radial basis function interpolation with either linear or Weighted Essentially Non Oscillatory (WENO) shape parameter approximation. When considered within Harten's framework for Multiresolution, these prediction operators give rise to sparse multi-scale representations of 2D signals, whose compression capabilities are demonstrated through numerical experiments. It is well know that the accuracy of multiquadric interpolation depends on the choice of the shape parameter. In addition, in [6], it was shown that the use of data-dependent strategies in the selection of the shape parameter leads to more accurate reconstructions. We shall show that our local adaptive estimates of the shape parameters lead to non-separable, fully 2D, reconstruction strategies that lead, in turn, to efficient compression algorithms.

1. Introduction

Image compression is a specific type of data compression whose aim is to reduce the amount of data necessary for image storage and transmission [13,24]. As such, it has an increasingly important role in applications such as remote sensing, videoconferencing, medical imaging and many more.

Many image compression algorithms rely on the use of classical wavelet based techniques, because they provide fast multi-scale decomposition/reconstruction algorithms which lead to sparse representations of an image when a thresholding strategy is applied to the multi-resolution representation of the data.

Among these techniques, compression algorithms based on *Harten's Multiresolution Framework* (HMRF) have some distinct advantages with respect to design and analysis. For example, the fact that the properties of the compression algorithm can easily be related to the properties of the basic reconstruction technique that is used to build the Prediction operators in the MR transformation has led to the development of the (nonlinear) ENO/WENO compression schemes in [3], which use the ENO or WENO nonlinear, piecewise polynomial reconstruction techniques [19,23], which are well known for being able to maximize the region where the reconstruction of piecewise smooth functions maintains its accuracy. These compression

☆ This research has been supported by Spanish MINECO project PID2020-117211GB-I00 and GVA project CIAICO/2021/227.
* Corresponding author.
E-mail addresses: arandiga@uv.es (F. Aràndiga), donat@uv.es (R. Donat), daniela.schenone25@gmail.com (D. Schenone).

https://doi.org/10.1016/j.amc.2023.128164
0096-3003/

schemes have demonstrated their increased compression capabilities, when edges are the dominant features in an image [1,3]. Other successful approaches to compression schemes within HRMF include the map-dependent approach described in [2], which can be considered as 'edge adapted' compression schemes.

The study carried out in this paper is motivated by the recent results presented in [6], where the authors analyze various reconstruction techniques based on locally scaled multi-quadric radial basis function (MQ-RBF) interpolation [11] for the reconstruction of discontinuous (1D) functions. It is shown in [6] that the local *shape parameter* can be *tuned* to obtain interpolatory reconstruction techniques that also maximize the region of high accuracy. The tuning considered in [6] involves an adaptive computation that incorporates techniques borrowed from (one-dimensional) WENO interpolation, which represent an improvement, in terms of approximation power, with respect to the MQ-RBF reconstruction techniques proposed in [14,15]. Since the accuracy of the reconstruction procedure has a direct impact on the size of the prediction errors, and hence on the compression capabilities of the associated MR transformation, in this paper, we shall design prediction operators within a non-tensor product 2D HMRF based on 2D version of the 1D MQ-RBF reconstruction techniques proposed in [6]. We shall examine the effect of different choices for the computation of the local shape parameters in the compression capabilities of the associated compression algorithms. In addition, we also consider the possibility of including in the design of the prediction operators information on the *edges* of the image. By computing an *edge map* of the image, we can also adapt the reconstruction process used in the design of the prediction operators to the local geometry of the image. We shall see that these *map-dependent approaches do increase*, the compression capabilities of the resulting MR transformation.

The outline of the paper is as follows: In Section 2 we recall the main notions regarding the mathematical tools used in the paper. In particular, Section 2.1 briefly presents Harten's interpolatory multi-resolution frameworks, and in Section 2.3 some basic notions about kernel interpolation with radial basis functions are presented. In Section 3 we present a local prediction step based on multiquadric RBF interpolation, while in Section 4 we focus on the design an analysis of suitable estimations for the local shape parameters, either by considering linear or WENO estimates. In Section 5 we present an alternative local prediction step for which the *centers* used for the MQ-RBF interpolation process are not centered around the interpolation point; this is a first step in order to design the map-aided MR transformations described in Sections 5 and 6. Finally, in Section 7 we present numerical comparisons between the proposed compression schemes, both with synthetic and real images.

2. Background knowledge

In this section we shall only cover the essential ingredients of HMRF and kernel Interpolation methods in order to make the paper 'essentially' self-contained. The reader is referred to [2,4,17] for further information on Harten's MRF, and to [6,11,12] for further information on kernel Interpolation techniques.

2.1. Harten's interpolatory MRF

Harten's MRF is specified by a sequence of triplets $(V_\ell, D_\ell^{\ell-1}, P_{\ell-1}^\ell)$, where V_ℓ is a finite-dimensional vector space and $\ell \in \mathbb{Z}$ is an index that specifies the level of resolution associated to V_ℓ. Here we shall assume that the level of resolution (hence the dimension of V_ℓ) decreases with ℓ. $D_\ell^{\ell-1} : V_{\ell-1} \to V_\ell$ (high to low resolution space) is called the *decimation operator* and $P_{\ell-1}^\ell : V_\ell \to V_{\ell-1}$ (low to high resolution space) is the *prediction operator*. The decimation operators define the framework, and they are often related to a particular class of *discretization operators* acting on suitable function spaces. In this paper we shall work within Harten's 2D point-value multi-resolution framework (MRF), where it is assumed that the discrete data sets $f^l \in V_\ell$ are 2-dimensional arrays (such as a gray-scale images, or the data associated to a 2D simulation on a discrete grid) which correspond to the point-values of a 2D function on an underlying grid which specifies the level of resolution attached to V_ℓ. Thus, if $f^0 \in V_0$, the finest resolution level in our context, corresponds to the point-values of an associated 2D function on an underlying uniform grid of $J_0 = (N_0+1)^2$ grid points, with $N_0 = 2^N$, the decimation operator in this point-value MRF is obtained by 2D-downsampling, i.e.

$$f^\ell_{2i,2j} = (D_\ell^{\ell-1} f^{\ell-1})_{2i,2j} = f^{\ell-1}_{i,j} \quad 0 \le i,j \le N_0 2^{-\ell}, \quad \ell \ge 0.$$

Hence f^ℓ is a $(N_0 2^{-\ell}+1)^2$ 2D array that corresponds to the point-values of the underlying function which generated f^0, on a uniform (ℓ-th level) grid of $J_\ell := (N_0 2^{-\ell}+1)^2$ points ($\dim V^\ell = J_\ell$).

The prediction operators in HMRF must satisfy the following *consistency* requirement with respect to the decimation operators:

$$D_\ell^{\ell-1} P_{\ell-1}^\ell f^\ell = f^\ell \qquad \forall f^\ell \in V_\ell. \tag{1}$$

In the interpolatory framework, (1) becomes

$$(D_\ell^{\ell-1}(P_{\ell-1}^\ell f^\ell))_{2i,2j} = f^\ell_{2i,2j} \quad 1 \le i,j \le N_0 2^{-\ell}+1 \tag{2}$$

which specifies that predicted values at even-even locations of the coarser grid are kept unchanged.

Notice that for all $f^{\ell-1} \in V^{\ell-1}$ we can write

$$f^{\ell-1} = P_{\ell-1}^\ell D_\ell^{\ell-1} f^{\ell-1} + e^{\ell-1}, \quad e^{\ell-1} := (I - P_{\ell-1}^\ell D_\ell^{\ell-1}) f^{\ell-1} \in V^{\ell-1}.$$

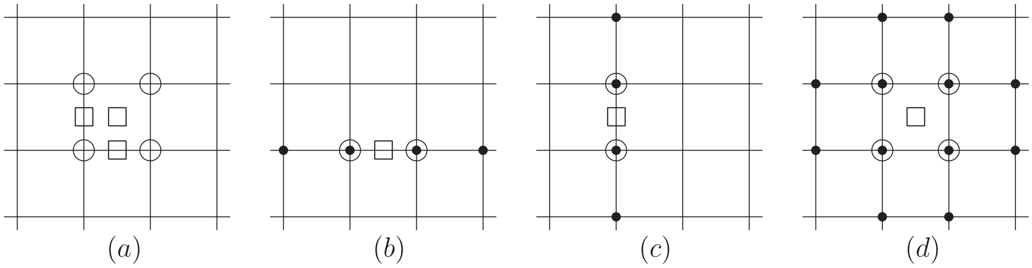

Fig. 1. (a) ◯ data at level ℓ, □ locations at level $\ell-1$ where detail coefficients are to be computed. (b)-(c)-(d) Reconstruction cases in Section 3. ◯ centers for the MQ-RBF interpolation. □ interpolation point. Interpolatory Prediction Stencils of Section 4.1 •. (b) Horizontal. (c) Vertical. (d) Diagonal.

Hence, the information contents of $f^{\ell-1}$ are equivalent to those in $(f^{\ell}, e^{\ell-1})$, where $f^{\ell} = D_{\ell}^{\ell-1} f^{\ell-1}$ is the *decimated* data at the next coarser level, and $e^{\ell-1} = f^{\ell-1} - P_{\ell-1}^{\ell} f^{\ell} \in V^{\ell-1}$ is the so-called *prediction error*.

Notice that, for each pair of indices (i, j), $0 \le i, j \le N_0 2^{-\ell}$, the *consistency* relation eq.(2) implies that $e_{2i,2j}^{\ell-1} = 0$. By storing the prediction errors at odd-odd (diagonal), odd-even (horizontal) and even-odd (vertical) locations, i.e. the three sets of *details*

$$\begin{cases} d_{2i,2j-1}^{\ell-1} := f_{2i,2j-1}^{\ell-1} - (P_{\ell-1}^{\ell} f^{\ell})_{2i,2j-1}, \\ d_{2i-1,2j}^{\ell-1} := f_{2i-1,2j}^{\ell-1} - (P_{\ell-1}^{\ell} f^{\ell})_{2i-1,2j}, \\ d_{2i-1,2j-1}^{\ell-1} := f_{2i-1,2j-1}^{\ell-1} - (P_{\ell-1}^{\ell} f^{\ell})_{2i-1,2j-1}, \end{cases} \qquad 1 \le i, j \le N_0 2^{-l},$$

together with the 'horizontal' and 'vertical' details for the first grid values

$$\begin{cases} d_{2i,2j-1}^{\ell-1} := f_{2i,2j-1}^{\ell-1} - (P_{\ell-1}^{\ell} f^{\ell})_{2i,2j-1}, & i = 0,\ 1 \le j \le N_0 2^{-\ell}, \\ d_{2i-1,2j}^{\ell-1} := f_{2i-1,2j}^{\ell-1} - (P_{\ell-1}^{\ell} f^{\ell})_{2i-1,2j}, & j = 0,\ 1 \le i \le N_0 2^{-\ell}, \end{cases}$$

we ensure a one-to-one correspondence between the sets (see Fig. 1-(a)),

$$\{f^{\ell-1}\} \equiv \{f^{\ell}, d^{\ell-1}\}.$$

In our context, if f^0 is an image of dimension $J_0 = (2^{N_0}+1)^2$, such that the gray level of a given pixel in the position $(m, n) \in [0, 2^{N_0}] \times [0, 2^{N_0}]$ is $f_{m,n}^0$, and we consider L resolution levels in the multi-resolution framework with $f^{\ell} := D_{\ell}^{\ell-1} f^{\ell-1}$, $1 \le \ell \le L$, repeating this two-scale process starting at the finest resolution level, we get an equivalent multi-scale decomposition of f^0, the finest resolution signal, in terms of a 'coarse' representation at the lowest resolution level f^L and a sequence of 'details'that include non-redundant information on the 'prediction errors' at all intermediate resolution levels,

$$\{f^0\} \equiv \{f^1, d^0\} \equiv \cdots \equiv \{f^L, d^{L-1}, \ldots . d^0\}.$$

MR-based compression algorithms work by setting to zero, or quantizing, small details in the MR representation of the original signal. Hence, the properties of the prediction operators used to obtain the above multiscale decomposition are crucial in order to obtain efficient (i.e. 'sparse'), multi-scale, compressed representations of fine-scale data.

Notice that (2) is an *interpolation condition* on the prediction operator, hence, in Harten's point-value (also called *interpolatory*) MRF, prediction operators may be constructed by considering interpolatory techniques for the approximation of a function from its point-values on a given grid. Since the details are interpolation errors, the efficiency of compression algorithms is directly related to the approximation properties of the interpolatory technique and the smoothness of the underlying function that provided the highest resolution data.

2.2. 2D Interpolatory prediction

In the 2D interpolatory MRF, to describe the prediction operator associated to a specific interpolatory technique it is sufficient to consider the following setting: Let $u : \Omega \subset \mathbb{R}^2 \to \mathbb{R}$, be a piecewise smooth function and $\mathcal{X} = \{p_{i,j}\}_{i,j \in \mathbb{Z}}$, $p_{i,j} = (x_i, y_j)$, a uniform grid of step-size h in both coordinate directions covering Ω. Given a pair of indices (i, j), the goal is to compute an approximation to $u(P)$ (see Fig. 1), for

- $P = (x_{i+\frac{1}{2}}, y_j)$ (Horizontal Approximation, HA),
- $P = (x_i, y_{j+\frac{1}{2}})$ (Vertical Approximation, VA),
- $P = (x_{i+\frac{1}{2}}, y_{,j+\frac{1}{2}})$ (Diagonal Approximation, DA).

Local interpolation techniques, in which the computation of the approximation to $u(P)$ involves only a stencil of interpolation points chosen as a convenient subset of $\{(x_{i+m}, y_{j+n})\}_{m,n=-p}^{q}$, for some $p, q \ge 1$, and the corresponding function values $u_{s,r} = u(x_s, y_r)$, are usually preferred.

Piecewise Polynomial Interpolation (PPI) provides classical examples of *local reconstruction techniques* which give rise to *local prediction operators*. Interpolatory MR decompositions based on data-independent PPI techniques have been considered in the literature [4,9,16].

In this case, the prediction operators are simply linear filters acting on the given data [4] and the behavior of the details at each resolution level depends on the stepsize of the underlying grid, as determined by the interpolation error formulas corresponding to the degree of the polynomial pieces used in the interpolation process [3].

Adaptivity was introduced in this context by considering ENO-WENO PPI. These techniques are able to maintain the accuracy of PP interpolants in a much larger region than their linear counterparts [3] and, as a consequence, ENO/WENO based compression algorithms outperform their linear counterparts in many situations of practical interest. It is worth mentioning that the stability of ENO-based compression algorithms with respect to perturbations needs a special approach [5], while WENO-based compression schemes are stable ([8]).

Prediction operators for the point-value 2D MRF can also be built using kernel Interpolation techniques. For the sake of completeness, we describe the essential ingredients of this type of interpolation next.

2.3. Kernel interpolation and radial basis functions.

The general setting for the *kernel interpolation* methods, is as follows: Let $K : \Omega \times \Omega \to \mathbb{R}$ be a symmetric *kernel*, defined on a domain $\Omega \subseteq \mathbb{R}^d$, and $P_1, \dots, P_N \subset \Omega$ a set of points in the domain, called *centers*. If the *kernel matrix* $A \in \mathbb{R}^{N\times N}$ with entries $A_{ij} := K(P_i, P_j),\ 1 \le i, j \le N$ is positive definite, then for the data

$$\mathcal{U} := \{U_1, \dots, U_N\} \quad \text{on data sites} \quad \mathcal{P} := \{P_1, \dots, P_N\}, \tag{3}$$

an interpolating function

$$S_{\mathcal{P},\mathcal{U}}(x) := \sum_{j=1}^{N} \lambda_j K(x, P_j) \tag{4}$$

can be completely determined by solving the linear system

$$A\lambda = \mathrm{U}, \quad \mathrm{U} = (U_1, \dots, U_N)^T, \tag{5}$$

which admits a unique solution. Kernels on $\mathbb{R}^d$ can be *scaled* by a positive factor ε, so obtaining a new kernel

$$K(x, y; \varepsilon) := K(x\varepsilon, y\varepsilon), \quad \forall x, y \in \mathbb{R}^d. \tag{6}$$

The parameter ε, called *shape parameter*, can be tuned by the user (according to the application) and plays an important role both for the accuracy of the interpolation method and its stability. The choice of a *good* shape parameter is a well–documented, problem-dependent issue (see [12] for a general review, and [7,25] for examples of particular approaches to this issue).

Radial kernels are translation invariant kernels of the form $K(x, y) := \Phi(x - y)$ where $\Phi(\cdot)$ is a *radial function*, i.e. $\Phi(x) = \phi(||x||_2)$, with $\phi : [0, \infty) \longrightarrow \mathbb{R}$ denoting a function of a single non-negative real variable and $||\cdot||_2$ the usual Euclidean norm. Scaled radial kernels obtained from the *multi quadric (MQ) radial function*

$$\phi(x) = \sqrt{1 + \varepsilon^2 x^2}, \tag{7}$$

have been recently considered for the local interpolation of one dimensional, possibly discontinuous, function in [6,14,15]. In [14,15], the authors show that the shape parameter can be *tuned* in order to enhance the accuracy of the RBF interpolant, and in [6], it is observed that it is possible to obtain accurate reconstructions both in smooth regions and in the vicinity of jump discontinuities by incorporating WENO adaptive techniques in the computation of the shape parameter.

3. Local prediction operators based on MQ-RBF interpolation

In this section we describe a simple prediction scheme based on a *parameter-dependent* kernel interpolation technique, as described in Section 2.3.

The required approximations to compute the prediction errors in the Horizontal, Vertical and Diagonal cases in Figure 1-(a) shall be computed using the scaled M-RBF function (7) and a set of centers which are symmetric with respect to the interpolation point, in each chosen direction (marked as ○ in Fig. 1-(b)-(c)-(d)).

Horizontal Approximation (vertical by symmetry). Considering the set of *centers* $\mathcal{P} = \{P_1, P_2\}$ with $P_1 = (x_i, y_j)$, $P_2 = (x_{i+1}, y_j)$, with associated data $u(P_l)$, $l = 1, 2$ (see Fig. 1-(a)), the MQ-RBF interpolant takes the form

$$R_H(x, y) = \sum_{m=1}^{2} \lambda_m \sqrt{1 + \varepsilon^2 ||(x, y) - P_m||_2^2}, \tag{8}$$

with $\lambda = [\lambda_1, \lambda_2]^T$ satisfying $A\boldsymbol{\lambda} = \mathbf{u}$, $(u_{m,n} = u(x_m, y_n))$

$$A = \begin{pmatrix} 1 & \sqrt{1+\varepsilon^2 h^2} \\ \sqrt{1+\varepsilon^2 h^2} & 1 \end{pmatrix}, \qquad \mathbf{u} = [u_{i,j}, u_{i+1,j}]^T.$$

After some straightforward algebra it is easy to arrive at the following expression

$$R_H(x_{i+\frac{1}{2}}, y_j) = \frac{u_{i,j} + u_{i,j+1}}{2} \frac{\sqrt{4 + h^2\varepsilon^2}}{1 + \sqrt{1 + h^2\varepsilon^2}},$$

and using a Taylor expansion around $x = 0$ of $\psi(x) = \frac{\sqrt{4+x^2}}{1+\sqrt{1+x^2}}$ we obtain

$$R_H(x_{i+\frac{1}{2}}, y_j) = \frac{u_{i,j} + u_{i,j+1}}{2}\left(1 - \frac{1}{8}h^2\epsilon^2 + \frac{11}{128}h^4\varepsilon^4\right) + O(h^6\varepsilon^6).$$

Assuming that u is sufficiently smooth, we readily deduce that $(u_{i+\frac{1}{2},j} = u(x_i + \frac{h}{2}, j))$

$$u(x_i + h/2, y_j) - R_H(x_{i+1/2}, y_j) = \frac{1}{8}(\varepsilon^2 u_{i+\frac{1}{2},j} - u''_{i+\frac{1}{2},j})h^2 + O(h^4). \tag{9}$$

Hence, choosing the shape parameter as

$$\varepsilon_H^2 := \frac{u''_{i+\frac{1}{2},j}}{u_{i+\frac{1}{2},j}} + O(h^p), \qquad p \geq 1, \tag{10}$$

the interpolation error can be expressed as follows

$$E^H_{i+\frac{1}{2},j}(\varepsilon_H) := u(x_i + h/2, y_j) - R_H(x_{i+1/2}, y_j) = O(h^{p+2}) + O(h^4) = O(h^{\min\{p+2,4\}}).$$

Thus, in smooth regions $E^H_{i+\frac{1}{2},j}(0) = O(h^2)$, and a second order approximation of the optimal shape parameter will provide the best possible approximation error, in the asymptotic sense. **Diagonal Approximation**. We consider as centers $\mathcal{P} = \{P_1, P_2, P_3, P_4\}$, with

$$P_1 = (x_i, y_j),\ P_2 = (x_{i+1}, y_j),\ P_3 = (x_{i+1}, y_{j+1}),\ P_4 = (x_i, y_{j+1}),$$

and the associated data $\{u_{i+m,j+n}\}_{m,n=0}^1$ (see Fig. 1-(d)) Then the MQ-RBF interpolant

$$R_D(x, y) = \sum_{m=1}^{4} \lambda_l \sqrt{1 + \varepsilon^2 ||(x, y) - P_m||_2^2} \tag{11}$$

where the coefficients λ_l are the solution of the linear system $A\boldsymbol{\lambda} = \mathbf{u}$ with

$$A = \begin{pmatrix} 1 & \sqrt{1+\varepsilon^2h^2} & \sqrt{1+2\varepsilon^2h^2} & \sqrt{1+\varepsilon^2h^2} \\ \sqrt{1+\varepsilon^2h^2} & 1 & \sqrt{1+\varepsilon^2h^2} & \sqrt{1+2\varepsilon^2h^2} \\ \sqrt{1+2\varepsilon^2h^2} & \sqrt{1+\varepsilon^2h^2} & 1 & \sqrt{1+\varepsilon^2h^2} \\ \sqrt{1+\varepsilon^2h^2} & \sqrt{1+2\varepsilon^2h^2} & \sqrt{1+\varepsilon^2h^2} & 1 \end{pmatrix}, \quad \mathbf{u} = \begin{bmatrix} u_{ij} \\ u_{i+1,j} \\ u_{i+1,j+1} \\ u_{i,j+1} \end{bmatrix}$$

takes the form

$$\begin{aligned} R_D(x_{i+\frac{1}{2},j} y_{j+\frac{1}{2}})) &= (\lambda_1 + \lambda_2 + \lambda_3 + \lambda_4)\sqrt{1 + \varepsilon^2\frac{h^2}{2}} \\ &= (u_{i,j} + u_{i+1,j} + u_{i+1,j+1} + u_{i,j+1})\frac{\sqrt{1 + \varepsilon^2\frac{h^2}{2}}}{1 + 2\sqrt{1+\varepsilon^2h^2} + \sqrt{1+2\varepsilon^2h^2}} \end{aligned}$$

and, using Taylor expansions as before

$$R_D(x_{i+\frac{1}{2}}, y_{j+\frac{1}{2}}) \quad = (u_{i,j} + u_{i+1,j} + u_{i+1,j+1} + u_{i,j+1})\left(\tfrac{1}{4} - \tfrac{1}{16}\varepsilon^2h^2 + \tfrac{9}{128}\varepsilon^4h^4\right) + O(\varepsilon^6h^6).$$

As in the previous cases, the approximation error can easily be estimated in smooth regions by using Taylor expansions of $u(x, y)$ around the evaluation point. Straightforward, but lengthy, computations lead to

$$E^D_{i+\frac{1}{2},j+\frac{1}{2}}(\varepsilon) \quad = u(x_{i+\frac{1}{2}}, y_{j+\frac{1}{2}}) - R_D(x_{i+\frac{1}{2}}, y_{j+\frac{1}{2}}) = \left(\tfrac{\varepsilon^2}{4}u - \tfrac{1}{8}u_{xx} - \tfrac{1}{8}u_{yy}\right)_{i+\frac{1}{2},j+\frac{1}{2}} h^2 + O(\epsilon^4h^4)$$

so that choosing (if possible, i.e. $u_{i+\frac{1}{2},j+\frac{1}{2}} \neq 0$)

$$\varepsilon_D^2 = \left(\frac{u_{xx} + u_{yy}}{2u}\right)_{i+\frac{1}{2},j+\frac{1}{2}} + O(h^p) \tag{12}$$

guarantees

$$E^D_{i+\frac{1}{2},j+\frac{1}{2}}(\epsilon_D) = O(h^{p+2}) + O(h^4) = O(h^{\min\{p+2,4\}}).$$

As before,under smoothness assumptions, $E^D_{i+\frac{1}{2},j+\frac{1}{2}}(0) = O(h^2)$, and a second order approximation of the optimal shape parameter is sufficient to ensure the optimal order in the interpolation error.

3.1. A Local MQ-RBF Prediction scheme.

Based on the asymptotic expansions and error analysis made in the previous section, the following parameter-dependent **local MQ-RBF-based prediction operators** ($\ell > 0$ is the resolution level, and f^ℓ the down-sampled image at level ℓ) lead to prediction errors that, under rather general smoothness conditions, can be of $O((h_\ell)^4)$:

Basic Prediction Formulas For $1 \le i, j \le N_0 2^{-l}$

$$\left\{\begin{array}{r} (P^\ell_{\ell-1} f^\ell)_{2i,2j-1} = (f^\ell_{i,j} + f^\ell_{i,j-1})\left(\frac{1}{2} - \frac{1}{16} h^2_\ell \varepsilon^2_{\ell,2i,2j-1}\right), \\ (P^\ell_{\ell-1} f^\ell)_{2i-1,2j} = (f^\ell_{i,j} + f^\ell_{i-1,j})\left(\frac{1}{2} - \frac{1}{16} h^2_\ell \varepsilon^2_{\ell,2i-1,2j}\right), \\ (P^\ell_{\ell-1} f^\ell)_{2i-1,2j-1} = (f^\ell_{i,j} + f^\ell_{i,j-1} + f^\ell_{i-1,j} + f^\ell_{i-1,j-1})\left(\frac{1}{2} - \frac{1}{16} h^2_\ell \varepsilon^2_{\ell,2i-1,2j-1}\right), \end{array}\right. \tag{13}$$

at the first grid locations at level ℓ, the 'horizontal' and 'vertical' predictions formulas are

$$(P^\ell_{\ell-1} f^\ell)_{2i,2j-1} = (f^\ell_{i,j} + f^\ell_{i,j-1})\left(\frac{1}{2} - \frac{1}{16} h^2_\ell \varepsilon^2_{\ell,2i,2j-1}\right),\ 1 \le j \le N_0 2^{-\ell},\ i = 0,$$

$$(P^\ell_{\ell-1} f^\ell)_{2i-1,2j} = (f^\ell_{i,j} + f^\ell_{i-1,j})\left(\frac{1}{2} - \frac{1}{16} h^2_\ell \varepsilon^2_{\ell,2i-1,2j}\right),\ 1 \le i \le N_0 2^{-\ell},\ j = 0.$$

The computation of the local shape parameters determines the accuracy of the prediction scheme (hence it also determines the efficiency of the associated compression scheme). Clearly, the computation of the shape parameters at each location must be carried out using the data available in a suitable neighborhood of the interpolation point and, to ensure the optimal accuracy under smoothness conditions, it is usually necessary to consider a data set which is larger than the set of *centers* used for the MQ-RBF interpolation process.

The *interpolatory prediction stencil (IPS)* (at each desired location at each resolution level) denotes the set of points/function values used in the basic prediction formulas. In all cases considered here, the IPS at a given location contains the set of centers used in the MQ-RBF interpolation process.

In the following section we consider and analyze different strategies to estimate the local shape parameters, that lead to different IPS and, thus, to prediction schemes with different approximation properties.

4. Parameter estimation strategies

If the underlying function u is sufficiently smooth, it is relatively simple to design linear strategies for the computation of the local shape parameters that attain the maximum asymptotic decay rate for the corresponding prediction errors. However, as observed in [6], when the function has discontinuous profiles, the use of these simple estimates leads to a complete loss of accuracy in the MQ-RBF interpolation technique and, hence, to large detail coefficients, in a wide band around the discontinuous profile. To reduce the region of low accuracy, the authors in [6] propose to use nonlinear strategies for the computation of the shape parameters inspired in the WENO technology. We examine next both strategies in the context of 2D MQ-RBF-MR-based compression. For simplicity in the description, we shall continue using notation in Section 2.2 throughout this section.

4.1. Linear strategies for the computation of the local shape parameters

Under smoothness conditions, second order centered approximations to the second order derivatives that appear in (10)-(12) lead to the desired optimal order in the interpolation errors. The resulting IPS are centered with respect to the interpolation point (• in Fig 1-(b)-(c)-(d)). **Horizontal Approximation (Vertical by symmetry)** The following 2D version of the linear estimate in Proposition 4.2 of [6],

$$\varepsilon^2_{\text{lin,H}} := \frac{u_{i-1,j} - u_{i,j} - u_{i+1,j} + u_{i+2,j}}{h^2(u_{i,j} + u_{i+1,j})} \tag{14}$$

satisfies, under smoothness assumptions,

$$\varepsilon^2_{\text{lin,H}} = \frac{u''_{i+\frac{1}{2},j}}{u_{i+\frac{1}{2},j}} + O(h^2) \quad \rightarrow \quad E^H_{i+\frac{1}{2},j}(\varepsilon^2_{lin,H}) = O(h^4). \tag{15}$$

However, if the function u has a discontinuity at $[x_{i-1}, x_{i+2}] \times y_j$, then we easily get

$$\varepsilon^2_{\text{lin,H}} = O(h^{-2}) \quad \rightarrow \quad E^H_{i+\frac{1}{2},j}(\varepsilon^2_{lin,H}) = O(1)$$

and, as a consequence the detail coefficient associated to the location associated to P is also $O(1)$. Hence, an isolated discontinuity in $[x_{i-1}, x_{i+1}] \times y_j$ produces a 'band ' of three large detail coefficients in the horizontal direction.

Diagonal. We follow a similar strategy, using second order centered approximations to derivatives and to the value of the function at the midpoint of a grid cell. For simplicity in the description we define the following auxiliary quantities,

$$\bar{u}_{i+\frac{1}{2},j+\frac{1}{2}} := \frac{1}{4}(u_{i,j}+u_{i+1,j}+u_{i,j+1}+u_{i+1,j+1}) \to u_{i+\frac{1}{2},j+\frac{1}{2}} = \bar{u}_{i+\frac{1}{2},j+\frac{1}{2}} + O(h^2).$$

$$(\bar{u}_{xx})_{i+\frac{1}{2},j+\frac{1}{2}} := \frac{1}{2h^2}(\bar{u}_{i-1,j+\frac{1}{2}} - \bar{u}_{i,j+\frac{1}{2}} - \bar{u}_{i+1,j+\frac{1}{2}} + \bar{u}_{i+2,j+\frac{1}{2}})$$
$$(\bar{u}_{yy})_{i+\frac{1}{2},j+\frac{1}{2}} := \frac{1}{2h^2}(\bar{u}_{i+\frac{1}{2},j-1} - \bar{u}_{i+\frac{1}{2},j} - \bar{u}_{i+\frac{1}{2},j+1} + \bar{u}_{i+\frac{1}{2},j+2})$$

with

$$\bar{u}_{i+m,j+\frac{1}{2}} = \frac{1}{2}(u_{i+m,j}+u_{i+m,j+1}), \quad \bar{u}_{i+\frac{1}{2},j+m} = \frac{1}{2}(u_{i,j+m}+u_{i+1,j+m}), \tag{16}$$

for $m=-1,0,1,2$. Again, under smoothness assumptions, taking into account that

$$\bar{u}_{i+m,j+\frac{1}{2}} = u_{i+m,j+\frac{1}{2}} + \frac{h^2}{2}u''_{i+m,j+\frac{1}{2}} + O(h^4), \quad \bar{u}_{i+\frac{1}{2},j+m} = u_{i+\frac{1}{2},j+m} + \frac{h^2}{2}u''_{i+\frac{1}{2},j+m} + O(h^4),$$

it is easy to prove that

$$(\bar{u}_{xx})_{i+\frac{1}{2},j+\frac{1}{2}} = (u_{xx})_{i+\frac{1}{2},j+\frac{1}{2}} + O(h^2), \quad (\bar{u}_{yy})_{i+\frac{1}{2},j+\frac{1}{2}} = (u_{yy})_{i+\frac{1}{2},j+\frac{1}{2}} + O(h^2),$$

hence

$$\varepsilon^2_{\text{lin,D}} := \frac{(\bar{u}_{xx})_{i+\frac{1}{2},j+\frac{1}{2}} + (\bar{u}_{yy})_{i+\frac{1}{2},j+\frac{1}{2}}}{2\bar{u}_{i+\frac{1}{2},j+\frac{1}{2}}} = \left(\frac{u_{xx}+u_{yy}}{2u}\right)(x_{i+\frac{1}{2}}, y_{j+\frac{1}{2}}) + O(h^2). \tag{17}$$

Therefore, under smoothness conditions, we get

$$E^D_{i+\frac{1}{2},j+\frac{1}{2}}(\varepsilon^2_{\text{lin,D}}) = O(h^4).$$

A similar accuracy loss occurs in the diagonal direction when there is a discontinuity that invalidates any of the approximation formulas used in the derivation above. In this case

$$\varepsilon^2_{\text{lin,D}} = O(h^{-2}) \quad \to \quad E^D_{i+\frac{1}{2},j+\frac{1}{2}}(\varepsilon^2_{lin,D}) = O(1)$$

which leads to a band of large prediction errors around isolated discontinuities and, as a consequence, to a reduction of the compression capabilities of the multiressolution transformation.

4.2. WENO-Like strategies for the computation of the local shape parameters

As observed in the 1D study carried out in [6], a more effective estimation for the optimal shape parameter can be obtained via adaptive WENO-like strategies. In this section, we shall provide WENO-type estimates for the shape parameters for MQ-RBF-interpolation of Section 3 and examine its effect on the accuracy of the MQ-RBF interpolation in the presence of discontinuities in the neighborhood if the interpolation point.

Horizontal Approximation (Vertical by symmetry) The starting point in our derivation are the following observations, which hold under smoothness conditions:

$$\bar{u}''_{i+\frac{1}{2},L} := \frac{u_{i-1,j} - 2u_{i,j} + u_{i+1,j}}{h^2} = u''_{i+\frac{1}{2},j} + O(h), \tag{18}$$

$$\bar{u}''_{i+\frac{1}{2},R} := \frac{u_{i,j} - 2u_{i+1,j} + u_{i+2,j}}{h^2} = u''_{i+\frac{1}{2},j} + O(h), \tag{19}$$

$$\frac{1}{2}\bar{u}''_{i+\frac{1}{2},L} + \frac{1}{2}\bar{u}''_{i+\frac{1}{2},R} = \frac{u_{i-1,j} - u_{i,j} - u_{i+1,j} + u_{i+2,j}}{2h^2} = u''_{i+\frac{1}{2},j+\frac{1}{2}} + O(h^2). \tag{20}$$

Notice that (18) holds when u is smooth on $[x_{i-1}, x_{i+1}] \times y_j$, (19) holds when u is smooth on $[x_i, x_{i+2}] \times y_j$, while (20) requires u to be smooth in $[x_{i-1}, x_{i+2}] \times y_j$ to hold.

Following the WENO-strategy of substituting the *optimal* weight coefficients (1/2, 1/2) in (20) by appropriate WENO-weights (Proposition 4.6 of [6]), we can easily define a second order WENO-like approximation for $u''_{i+\frac{1}{2},j}$ as follows:

$$\mathcal{I}_\ell := \frac{13}{12}(u_{i-1,j} - 2u_{i,j} + u_{i+1,j})^2 + \frac{1}{4}(u_{i-1,j} - 4u_{i,j} + 3u_{i+1,j})^2,$$
$$\mathcal{I}_r := \frac{13}{12}(u_{i,j} - 2u_{i+1,j} + u_{i+2,j})^2 + \frac{1}{4}(u_{i+2,j} - u_{i,j})^2,$$

$$\alpha_\ell := \frac{1}{2(h^2+\mathcal{I}_\ell)^2}, \quad \alpha_r := \frac{1}{2(h^2+\mathcal{I}_r)^2}, \quad w_\ell := \frac{\alpha_\ell}{\alpha_\ell+\alpha_r}, \quad w_r := \frac{\alpha_r}{\alpha_\ell+\alpha_r},$$

$$\varepsilon^2_{wen,H} := \frac{w_\ell\, \bar{u}''_{i+\frac{1}{2},j,L} + w_r\, \bar{u}''_{i+\frac{1}{2},j,R}}{(u_{ij}+u_{i+1,j})/2}. \tag{21}$$

With the same techniques used in [6], it is easy to show that the interpolation error is $O(1)$ only at the interval where the discontinuity is located:

1. If u is smooth on $[x_{i-1},x_{i+2}]\times[y_j]$, then $E^H_{i+\frac{1}{2},j}(\varepsilon^2_{wen,H}) = O(h^4)$.
2. If u has a discontinuity in $[x_{i-1},x_i]\times y_j$, or in $[x_{i+1},x_{i+2}]\times y_j$, then $E^H_{i+\frac{1}{2},j}(\varepsilon^2_{wen,H}) = O(h^3)$.

Diagonal Approximation Taking into account (16) and the derivation in Section 4.1, we can write

$$\begin{aligned}\frac{\bar{u}_{i-1,j+\frac{1}{2}} - \bar{u}_{i,j+\frac{1}{2}} - \bar{u}_{i+1,j+\frac{1}{2}} + \bar{u}_{i+2,j+\frac{1}{2}}}{2h^2} &= \frac{1}{2}\frac{\bar{u}_{i-1,j+\frac{1}{2}} - 2\bar{u}_{i,j+\frac{1}{2}} + \bar{u}_{i+1,j+\frac{1}{2}}}{h^2}\\ &+ \frac{1}{2}\frac{\bar{u}_{i,j+\frac{1}{2}} - 2\bar{u}_{i+1,j+\frac{1}{2}} + \bar{u}_{i+2,j+\frac{1}{2}}}{h^2},\end{aligned}$$

$$\begin{aligned}\frac{\bar{u}_{i+\frac{1}{2},j-1} - \bar{u}_{i+\frac{1}{2},j} - \bar{u}_{i+\frac{1}{2},j+1} + \bar{u}_{i+\frac{1}{2},j+2}}{2h^2} &= \frac{1}{2}\frac{(\bar{u}_{i+\frac{1}{2},j-1} - 2\bar{u}_{i+\frac{1}{2},j} + \bar{u}_{i+\frac{1}{2},j+1})}{h^2}\\ &+ \frac{1}{2}\frac{(\bar{u}_{i+\frac{1}{2},j} - 2\bar{u}_{i+\frac{1}{2},j+1} + \bar{u}_{i+\frac{1}{2},j+2})}{h^2}.\end{aligned}$$

Hence, we can apply again the same WENO-like strategy as before, by defining appropriate smoothness estimators as follows:

$$\begin{aligned}
\mathcal{I}^x_\ell &:= \frac{13}{12}(\bar{u}_{i-1,j+\frac{1}{2}} - 2\bar{u}_{i,j+\frac{1}{2}} + \bar{u}_{i+1,j+\frac{1}{2}})^2 + \frac{1}{4}(\bar{u}_{i-1,j+\frac{1}{2}} - 4\bar{u}_{i,j+\frac{1}{2}} + 3\bar{u}_{i+1,j+\frac{1}{2}})^2,\\
\mathcal{I}^x_r &:= \frac{13}{12}(\bar{u}_{i,j+\frac{1}{2}} - 2\bar{u}_{i+1,j+\frac{1}{2}} + \bar{u}_{i+2,j+\frac{1}{2}})^2 + \frac{1}{4}(\bar{u}_{i+2,j+\frac{1}{2}} - \bar{u}_{i,j+\frac{1}{2}})^2,\\
\mathcal{I}^y_\ell &:= \frac{13}{12}(\bar{u}_{i+\frac{1}{2},j-1} - 2\bar{u}_{i+\frac{1}{2},j} + \bar{u}_{i+\frac{1}{2},j+1})^2 + \frac{1}{4}(\bar{u}_{i+\frac{1}{2},j-1} - 4\bar{u}_{i+\frac{1}{2},j} + 3\bar{u}_{i+\frac{1}{2},j+1})^2,\\
\mathcal{I}^y_r &:= \frac{13}{12}(\bar{u}_{i+\frac{1}{2},j} - 2\bar{u}_{i+\frac{1}{2},j+1} + \bar{u}_{i+\frac{1}{2},j+2})^2 + \frac{1}{4}(\bar{u}_{i+\frac{1}{2},j+2} - \bar{u}_{i+\frac{1}{2},j})^2,
\end{aligned}$$

$$\alpha^z_\ell := \frac{1}{2(h^2+\mathcal{I}^z_\ell)^2}, \quad \alpha^z_r := \frac{1}{2(h^2+\mathcal{I}^z_r)^2}, \quad w^z_\ell := \frac{\alpha^z_\ell}{\alpha^z_\ell+\alpha^z_r}, \quad w^z_r := \frac{\alpha^z_r}{\alpha^z_\ell+\alpha^z_r}, \quad z = x, y,$$

$$\varepsilon^2_{wen,D} := \frac{w^x_\ell(\bar{u}_{i-1,j+\frac{1}{2}} - 2\bar{u}_{i,j+\frac{1}{2}} + \bar{u}_{i+1,j+\frac{1}{2}}) + w^x_r(\bar{u}_{i,j+\frac{1}{2}} - 2\bar{u}_{i+1,j+\frac{1}{2}} + \bar{u}_{i+2,j+\frac{1}{2}})}{h^2 2\bar{u}_{i+\frac{1}{2},j+\frac{1}{2}}} \tag{22}$$

$$+\frac{w^y_\ell(\bar{u}_{i+\frac{1}{2},j-1} - 2\bar{u}_{i+\frac{1}{2},j} + \bar{u}_{i+\frac{1}{2},j+1}) + w^y_r(\bar{u}_{i+\frac{1}{2},j} - 2\bar{u}_{i+\frac{1}{2},j+1} + \bar{u}_{i+\frac{1}{2},j+2})}{h^2 2\bar{u}_{i+\frac{1}{2},j+\frac{1}{2}}}. \tag{23}$$

Straightforward, but lengthy, computations lead to

1. If u is smooth on $[x_{i-1},x_{i+2}]\times[y_{j-1},y_{j+2}]$, then $E^H_{i+\frac{1}{2},j+\frac{1}{2}}(\varepsilon^2_{wen,D}) = O(h^4)$.
2. if u is smooth but for an isolated discontinuity curve located in one and only one of the following regions: $[x_{i-1},x_i]\times[y_{j-1},y_{j+2}]$, $[x_{i+1},x_{i+2}]\times[y_{j-1},y_{j+2}]$, $[x_{i-1},x_{i+2}]\times[y_{j-1},y_j]$, $[x_{i-1},x_{i+2}]\times[y_{j+1},y_{j+2}]$, then $E^D_{i+\frac{1}{2},j+\frac{1}{2}}(\epsilon_{wen,D}) = O(h^3)$.

Hence, for sufficiently isolated discontinuities, the loss of accuracy is, again, restricted to the grid cell that contains the discontinuity.

5. Map dependent local reconstruction and parameter estimation

The design of nonlinear prediction schemes in the previous section relies on WENO strategies in order to choose IPS that *move away* from discontinuity curves. Similar nonlinear (i.e. data-dependent) strategies can be considered if an *edge map* of the image is available. In this section we present a map-dependent local prediction scheme which uses the information given by a previously constructed *edge map* of the image in order to choose the IPS at each interpolation point and each resolution level.

The first step in this algorithm is the construction of a binary edge map that contains information on the location of the discontinuities in the image. The edge map is required to have two pixels for each 'detected' discontinuity, one before and one following the luminosity change in the image.

A simple computation of an appropriate edge map at the finest resolution level is carried out in the following three steps.

Step 1. At a given location on the finest grid, compute the horizontal and vertical gradient of the image and an edge map with the *Sobel edge detection algorithm* ([20,21]).

Step 2. For both horizontal and vertical gradients, we define as edge points couples of consecutive pixels obtained with the Sobel edge detection algorithm such that the sum of their respective gradient values is greater than the sum of the 4-adjacent gradient values.

Step 3 The remaining marked points are chained one to the other using North-East-South-West (NESW) chain codes [10], as it is done in [2]. A control of the length of the obtained chains is performed and, according to a threshold, L_{chain}, leads to a rejection from the map of the marked points belonging to chains of length smaller than L_{chain}. We take $L_{chain} \in [20, 120]$ pixels, depending on the size and the geometry of the image. To be able to define the sequence of map-dependent prediction operators, we need to compute the edge map corresponding to each resolution level. The following sketch provides the code for obtaining the edge map at each level.

1. input: Let m^0 be the binary edge image at the finest level, and L the number of levels
2. for $\ell = 0 : L-1$ do
   (a) if $m^{\ell}_{i,j} = 1$ and $m^{\ell}_{i,j+1} = 1$ then
      (1) If i is even then
         (1) If j is even, then $m^{\ell+1}_{\frac{i}{2},\frac{j}{2}} = 1$ and $m^{\ell+1}_{\frac{i}{2},\frac{j}{2}+1} = 1$.
         (2) If j is odd, then $m^{\ell+1}_{\frac{i}{2},\frac{j+1}{2}-1} = 1$ and $m^{\ell+1}_{\frac{i}{2},\frac{j+1}{2}} = 1$
      (2) If i is odd then
         (1) If j is even, then $m^{\ell+1}_{\frac{i-1}{2}-1,\frac{j}{2}} = 1$ and $m^{\ell+1}_{\frac{i-1}{2},\frac{j}{2}+1} = 1$.
         (2) If j is odd, then $m^{\ell+1}_{\frac{i-1}{2}-1,\frac{j+1}{2}-1} = 1$ and $m^{\ell+1}_{\frac{i-1}{2},\frac{j+1}{2}} = 1$
   (b) end
3. end
4. output: m^{ℓ}, $\ell = 0, \dots, L$, maps at each compression level

Proceed analogously when $m^{\ell}_{i,j} = 1$ and $m^{\ell}_{i+1,j} = 1$, switching the roles of i and j.

The edge maps serve to *separate* the *smoothness regions* in the image at each resolution level. This information can be used to chose IPS that *move away* from the discontinuity curves (contours) in the image. We exemplify some instances of this process in the following section.

5.1. Map-dependent MQ-RBF interpolation

The basic idea behind our map-dependent interpolation procedure is as follows: in a smooth region of the image, the centered choice of IPS described in Section 4.1 guarantees the optimal order in the interpolation error, and should be adopted, but if the centered IPS *crosses* a discontinuity, a non-centered IPS selection should be adopted instead, in order to maintain at least some accuracy in the approximation. Obviously, the *best IPS* selection at each location and resolution level will depend on the *orientation* of the family of edge maps. The general procedure is given in Section 5.2, and it is based on considering MQ-RBF extrapolation for the approximation of the required values, as explained in the next subsection, where we exemplify the process by describing two particular cases.

5.1.1. Horizontal (vertical by symmetry)

Consider the case displayed in Fig. 2 (top-left). Here, according to the information contained in the edge map, the set of centers for the MQ-RBF interpolation must be located to the right the approximation point, in order to keep all of them on the *same* smoothness region of the function.

For this situation, and using the notation of Section 3, the corresponding MQ-RBF interpolating function uses the set of centers displayed in Fig. 2 (top-right), which is given by

$$R_2(x, y) = \sum_{m=1}^{2} \lambda_i \sqrt{1 + \varepsilon^2\left((x - x_{i+m})^2 + (y - y_j)^2\right)}. \tag{24}$$

Proceeding as in Section 3, we arrive at the following expression for the interpolation error

$$E(P^c) = \frac{3}{8}(u_{i+\frac{1}{2},j}\varepsilon^2 - u''_{i+\frac{1}{2},j})h^2 + \frac{1}{4}(u'''_{i+\frac{1}{2},j} - 3u'_{i+\frac{1}{2},j}\varepsilon^2)h^3 + O(h^4),$$

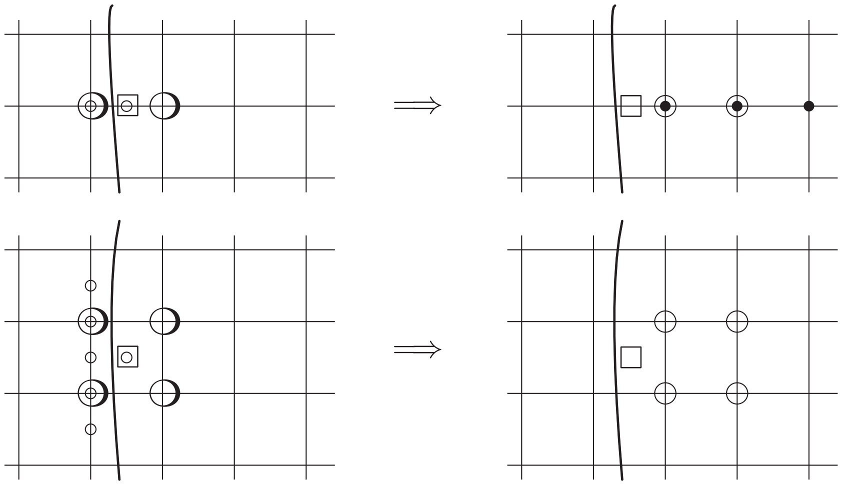

Fig. 2. Map dependent prediction of Section 5.1. Top Row: Horizontal case. Bottom Row: Diagonal case. Left Column: the ❍ symbol denotes edge points at level ℓ, the $\circ$ symbol denotes edge points at level $\ell-1$. Right Column: ◯ denotes MQ-RBF centers used to approximate at □.

Fig. 3. Original 513×513 pixel images.

so that

$$\varepsilon^2 := \frac{u''_{i+\frac{1}{2},j}}{u_{i+\frac{1}{2},j}} + O(h^p) \quad \rightarrow \quad E(P^c) = O(h^{\min\{2+p,3\}}).$$

Hence, by choosing a *sided* set of centers, we can still achieve a third order approximation.

By using Taylor expansions, we easily get that

$$R_2(x_{i+\frac{1}{2}}, y_j) = \left(-\frac{1}{2} + \frac{9}{16}\varepsilon^2 h^2\right)u_{i+2,j} + \left(\frac{3}{2} - \frac{3}{16}\varepsilon^2 h^2\right)u_{i+1,j} + O(h^3), \tag{25}$$

and an appropriate selection of the shape parameter, using function values from the smoothness region, could be as follows

$$\varepsilon^2_{H,R} := \frac{(u_{i+1,j} - 2u_{i+2,j} + u_{i+3,j})/2}{h^2(3u_{i+1} - u_{i+2})/2} = \frac{u''_{i+\frac{1}{2},j}}{u_{i+\frac{1}{2},j}} + O(h) \quad \rightarrow \quad E_{i+\frac{1}{2},j}(\varepsilon_{H,R}) = O(h^3).$$

The resulting IPS at the location of P^c would then be $\{x_{i+1}, x_{i+2}, x_{i+3}\} \times y_j$ and the prediction formula would consider the first two terms in (25).

It is worth noticing that $E_{i+\frac{1}{2},j}(0) = O(h^2)$, which only requires $\{x_{i+1}, x_{i+2}\} \times y_j$ as the IPS, i.e. the set of centers used for the MQ-RBF extrapolation.

5.1.2. Diagonal

Consider now the case shown in Fig. 2 (bottom). To keep the approximation point and the set of centers in the MQ-RBF interpolation process on the *same smoothness region*, we need to consider the set of centers $\{(x_{i+1}, y_j), (x_{i+1}, y_{j+1}), (x_{i+2}, y_j), (x_{i+2}, y_{j+1})\}$. In this case, the lack of symmetry with respect to the interpolatory point leads to rather complicated asymptotic expressions which, in addition, require quite involved formulas for the determination of the shape parameter (within smooth regions). To keep the formulas as simple as possible, we use only the 0-th order terms (i.e. setting $\varepsilon = 0$), which in this case leads to

$$R_4(x_i + h/2, y_i + h/2) = \frac{3}{4}u_{i+1,j} - \frac{1}{4}u_{i+2,j} - \frac{1}{4}u_{i+2,j+1} + \frac{3}{4}u_{i+1,j+1} + O(h^2), \tag{26}$$

i.e. $E_{i+\frac{1}{2},j+\frac{1}{2}}(0) = O(h^2)$, and use the first four terms in (26) in the prediction formulas.

Obviously, the determination of a 4-point set of centers (which is also the IPS) in a smooth region in the diagonal case is much more complex than in the Horizontal/Vertical cases, but can be done taking into account the edge maps at consecutive resolution levels and the *orientation* of the edges. We sketch our *map-dependent prediction* operators next.

5.2. Map-dependent prediction

The idea is to use the edge maps at each resolution level to choose an *oriented IPS* at each required location and each resolution level, which shall be used to compute the MQ-RBF prediction.

In order to decide the appropriate approximation formula at each location, we use first the edge maps to decide if an edge crosses the symmetric 2-point (horizontal and vertical) or the 4-point (diagonal) set of centers used the **basic prediction** of Section 3.1 (the centers of the MQ-RBF interpolation are *centered* with respect to the prediction point). If this is the case, an oriented IPS selection, and corresponding approximation formula is required. For this, we analyze how the other edge points around the approximation point are distributed and we check the local discrete tangent versor for each edge point (this computation can be easily performed by using the MATLAB function `regionprops`) ([21,22]).

A sketch of the code used for the process is provided next.

Let $\ell > 0$ be the compression level we are at. Our aim is to reconstruct level ℓ.

1. Horizontal case (symmetrically for the vertical case): the aim is to determine the local reconstruction at $(x_{i+\frac{1}{2}}, y_j)$
   (a) if $m^{\ell+1}_{i,j} = m^{\ell+1}_{i+1,j} = 1$
   (are edges of the $(\ell+1)$th level map)
   we consider the map at level ℓ
   (1) if $m^{\ell}_{2i,2j} = m^{\ell}_{2i+1,2j} = 1$
   and $m^{\ell}_{2i+2,2j} = 0$: (x_i, y_j) and $(x_{i+\frac{1}{2}}, y_j)$ are edges and (x_{i+1}, y_j) is not: use the set of centers $\{(x_{i+1}, y_j), (x_{i+2}, y_j)\}$ to compute the MQ-RBF approximation. ((25) and Fig. 2 (top))
   if $m^{\ell}_{2i+1,2j} = m^{\ell}_{2i+2,2j} = 1$
   and $m^{\ell}_{2i,2j} = 0$:
   use the set of centers $\{(x_{i-1}, y_j), (x_i, y_j)\}$ to compute the MQ-RBF approximation,
   else use **Basic Prediction Formulas** (13) (i.e. the set of centers is $\{(x_i, y_j), (x_{i+1}, y_j)\}$
   (b) else we use **Basic Prediction Formulas** (13)
2. Diagonal case, the aim is to compute the local reconstruction at $(x_{i+\frac{1}{2}}, y_{j+\frac{1}{2}})$
   (a) we consider the map at level $\ell + 1$,
   (b) if $m^{\ell+1}_{i,j} = m^{\ell+1}_{i+1,j} = m^{\ell+1}_{i,j+1} = m^{\ell+1}_{i+1,j+1} = 1$
   we consider the map at level ℓ, and we compute the reconstruction as follows:
   (1) if $m^{\ell}_{2i+1,2j+1} = 1$ and $\sum_{s=2j-1}^{2j+3} m^{\ell}_{2i,s} \geq 3$, and the angle of the discrete normal versor $\mathbf{v}_{i+\frac{1}{2},j+\frac{1}{2}}$ of the edge in $m^{\ell}_{2i+1,2j+1} = 1$ is in $[\frac{\pi}{4}, \frac{3\pi}{4}] \cup [\frac{5\pi}{4}, \frac{7\pi}{4}]$: we use the centers $\{(x_{i+1}, y_j), (x_{i+1}, y_{j+1}), (x_{i+2}, y_j), (x_{i+2}, y_{j+1})\}$ ((26) and Fig. 2 (bottom)),
   if $m^{\ell}_{2i+1,2j+1} = 1$ and $\sum_{s=2j-1}^{2j+3} m^{\ell}_{2i+2,s} \geq 3$, and the angle of the discrete normal versor $\mathbf{v}_{i+\frac{1}{2},j+\frac{1}{2}}$ of the edge in $(x_{i+\frac{1}{2}}, y_{j+\frac{1}{2}})$ is in $[\frac{\pi}{4}, \frac{3\pi}{4}] \cup [\frac{5\pi}{4}, \frac{7\pi}{4}]$: we use the stencil $\{(x_i, y_j), (x_i, y_{j+1}), (x_{i-1}, y_j), (x_{i-1}, y_{j+1})\}$,
   if $m^{\ell}_{2i+1,2j+1} = 1$ and $\sum_{s=2i-1}^{2i+3} m^{\ell}_{s,2j} \geq 3$, and the angle of the discrete normal versor $\mathbf{v}_{i+\frac{1}{2},j+\frac{1}{2}}$ of the edge in $(x_{i+\frac{1}{2}}, y_{j+\frac{1}{2}})$ is in $[-\frac{\pi}{4}, \frac{\pi}{4}] \cup [\frac{3\pi}{4}, \frac{5\pi}{4}]$: we use the stencil $\{(x_i, y_{j+1}), (x_i, y_{j+2}), (x_{i+1}, y_{j+1}), (x_{i+1}, y_{j+2})\}$,
   if $m^{\ell}_{2i+1,2j+1} = 1$ and $\sum_{s=2i-1}^{2i+3} m^{\ell}_{s,2j+2} \geq 3$, and the angle of the discrete normal versor $\mathbf{v}_{i+\frac{1}{2},j+\frac{1}{2}}$ of the edge in $(x_{i+\frac{1}{2}}, y_{j+\frac{1}{2}})$ is in $[-\frac{\pi}{4}, \frac{\pi}{4}] \cup [\frac{3\pi}{4}, \frac{5\pi}{4}]$: we use the stencil $\{(x_i, y_j), (x_i, y_{j-1}), (x_{i+1}, y_j), (x_{i+1}, y_{j-1})\}$,
   else we use **Basic Prediction Formulas** (13)
   (c) else we use **Basic Prediction Formulas** (13)

6. Map-building prediction

In this section we present the different map-aided prediction strategy, also based on the error analysis of the various local multiquadric-RBF interpolatory techniques considered in this paper.

The basic idea for this method is to check which IPS/prediction formula is better suited to carry out the local reconstruction at each point on each resolution level, on the decomposition step of the MR transformation. This involves determining

Table 1
Outcomes of different image compression methods applied to the image of Fig. 3(a). Comparisons in terms of number of non-zero elements, bytes and PSNR.

type	L	q	nnz		bytes		PSNR
			details	**map**	**details**	**map**	
lin	3	32	5365	0	4087	0	34.73
lin	3	64	4560	0	3431	0	32.30
lin	3	128	1118	0	1632	0	25.48
WENO	3	32	5232	0	4028	0	38.33
WENO	3	64	4512	0	3459	0	34.87
WENO	3	128	1094	0	1581	0	25.81
WENO map	3	32	690	7696	1379	774	49.43
WENO map	3	64	576	7606	1176	774	42.25
WENO map	3	128	257	7696	689	774	36.71
WENO map-b.	3	32	47	4550	402	679	47.36
WENO map-b.	3	64	30	4550	375	679	45.79
WENO map-b.	3	128	15	4550	363	679	44.27

Table 2
Outcomes of different image compression methods applied to the image of Fig. 3(b). Comparisons in terms of number of non-zero elements, bytes and PSNR.

type	L	q	nnz		bytes		PSNR
			details	**map**	**details**	**map**	
lin	3	32	8936	0	7284	0	31.06
lin	3	64	2873	0	2998	0	27.88
lin	3	128	504	0	923	0	24.72
WENO	3	32	9087	0	7686	0	31.83
WENO	3	64	3069	0	3308	0	28.50
WENO	3	128	502	0	885	0	25.04
WENO map	3	32	8331	3455	6992	700	31.80
WENO map	3	64	2388	3455	2695	700	28.56
WENO map	3	128	370	3455	776	700	25.91
WENO map-b.	3	32	4678	4974	4744	2222	31.39
WENO map-b.	3	64	755	4974	1236	2222	29.36
WENO map-b.	3	128	121	4974	458	2222	28.17

which reconstruction technique, among a (small) set of those considered in the previous sections provides the smallest prediction error at each location/resolution level. To implement this strategy, we compare the prediction errors obtained from the reconstruction with centered stencil where the IPS are obtained using WENO (**Basic Prediction Formulas**) of Sections 3–4 with those obtained from several different reconstructions with non-centered stencils: Two each for horizontal (Figure 2, top right) and vertical cases, and four for the diagonal case (Figure 2 bottom right). Then and finally we select the one which provides the smallest prediction error, keeping the IPS/prediction formula identified in a *map*, which is being built along with the decomposition step. The entries of the map are $\{0, 1, \ldots, 4\}$, where 0 represent centered points reconstruction and 1 to 4 the other options. The information stored in the map is then used in the reconstruction of the image after compression takes place.

7. Numerical experiments

In this Section we compare the efficiency of the compression algorithms associated to our methods on two different types of images: a synthetic image and the *peppers* photographic image, displayed in Fig. 3.

The algorithms used in the prediction operators that define the MR transformation are the following

- pure linear and WENO methods (Sections 3–4)
- map-dependent method with WENO parameter estimation (Section 5)
- map-building method with WENO parameter estimation (Section 6)

In each case, we take $L = 3$ and three different quantization parameters $q = 32, 64, 128$ for compression purposes. The comparisons, presented in Tables 1 and 2, take into account

- the number of non zero details (and eventually non-zero map entries) and the number of bytes that are required to store them,
- the *quality* of the reconstructed image, after compression takes place, measured by the Peak Signal-to-Noise Ratio (PSNR) [18].

The tables show that the map aided methods outperform the pure linear and WENO methods, and this is especially evident for synthetic images, where the edges are more pronounced. We also find that even when the linear methods have

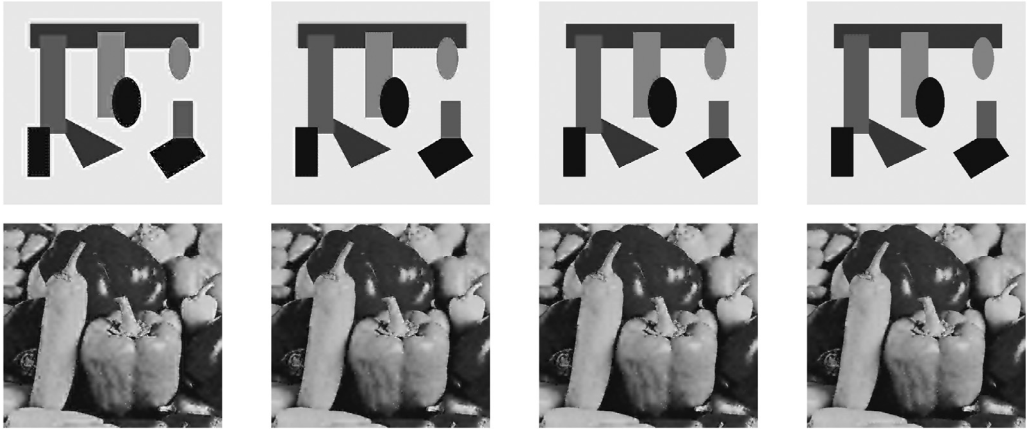

Fig. 4. Decompressed images, with $L = 3$ and $q = 64$. First column: LINEAR parameter esimation. Second: WENO parameter estimation. Third: map dependent method with WENO parameter estimation. Fourh: map-building method with WENO parameter estimation.

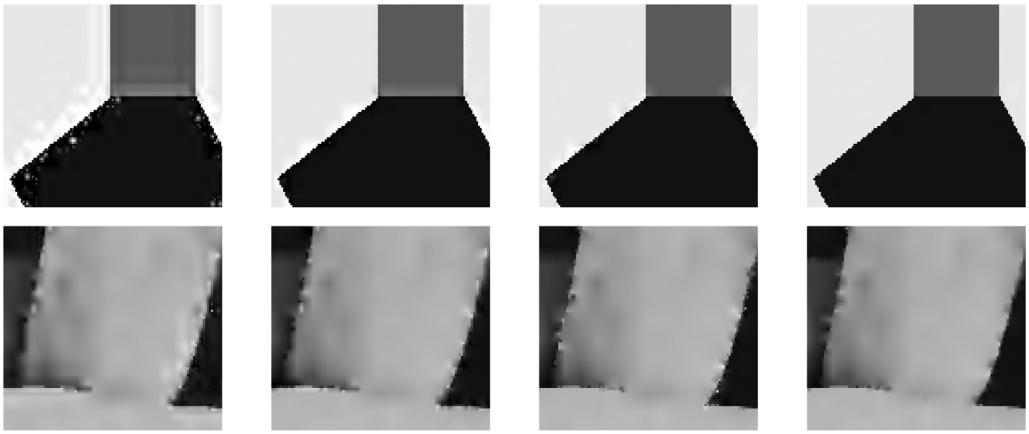

Fig. 5. Zoom of decompressed images, with $L = 3$ and $q = 64$. First column: LINEAR parameter estimation. Second: WENO parameter estimation. Third: map dependent method with WENO parameter estimation. Fourh: map-building method with WENO parameter estimation.

compression ratios which are comparable with the WENO methods, with the latter, the reconstructed image has better *visual quality*, as can be observed in Figs. 4 and 5.

Data availability

No data was used for the research described in the article.

References

[1] S. Amat, F. Aràndiga, A. Cohen, R. Donat, Tensor product multiresolution analysis with error control for compact image representation, Signal Process 82 (2) (2002) 587–608.
[2] F. Aràndiga, J. Baccou, M. Doblas, J. Liandrat, Image compression based on a multi-directional map-dependent algorithm, Appl. Comput. Harmon. Anal. 23 (2) (2007) 181–197.
[3] F. Aràndiga, A.M. Belda, P. Mulet, Point-value weno multiresolution applicarions to stable image compression, J. Sci. Comp. 43 (2) (2010) 158–182.
[4] F. Aràndiga, R. Donat, Nonlinear multiscale decompositions: the approach of A. Harten, Numer. Algorithms 23 (2) (2000) 175–216.
[5] F. Aràndiga, R. Donat, Stability through syncronization in nonlinear multiscale transformations, SIAM J. Sci. Comput. 29 (1) (2007) 265–289.
[6] F. Aràndiga, R. Donat, L. Romani, M. Rossini, On the reconstruction of discontinuous functions using multiquadric rbf-weno local interpolation techniques, Math. Comput. Simul. 176 (2020) 4–24.
[7] R. Cavoretto, A. Rossi, M.S. Mukhametzhanov, Y.D. Sergeyev, On the search of the shape parameter in radial basis functions using univariate global optimization methods, J. Glob. Optim. 79 (2021) 305–327.
[8] A. Cohen, N. Dyn, B. Matei, Quasilinear subdivision schemes with applications to ENO interpolation, Appl. Comput. Harmon. Anal. 15 (2003) 89–116.
[9] D.L. Donoho, Interpolating wavelet transforms, Technical Report, Department of Statistics, Stanford University, 1992.
[10] R.R. Estes, R. Algazi, Efficient error chain coding of binary documents 3 (1993) 122–131.
[11] G.E. Fasshauer, Meshfree approximation methods with matlab, Interdiscip. Math. Sci. 6 (2007).
[12] G.E. Fasshauer, J.G. Zhang, On choosing "optimal"shape parameters for rbf approximation, Numer. Algor. 45 (1–4) (2007) 345–368.
[13] R.C. Gonzalez, R.E. Woods, Digital Image Processing, Prentice Hall, 2002. 2nd Ed.

[14] J. Guo, J.-H. Jung, Radial basis function eno and weno finite difference methods based on the optimization of shape parameters, J. Sci. Comp. 70 (2) (2017) 551–575.
[15] J. Guo, J.-H.A. Jung, Plx, Rbf-weno finite volume method for hyperbolic conservation laws with the monotone polynomial interpolation method, Appl. Numer. Math. 112 (2017) 27–50.
[16] A. Harten, Discrete multiresolution analysis and generalized wavelets, Appl. Num. Math. 12 (1993) 153–193.
[17] A. Harten, Multiresolution representation of data: a. general framework, SIAM J. Numer. Anal. 33 (3) (1996) 1205–1256.
[18] Q. Huynh-Thu, M. Ghanbari, Scope of validity of psnr in image/video quality assessment, Electron. Lett. 44 (13) (2008) 800–801.
[19] G.S. Jiang, C.W. Shu, Efficient implementation of weighted eno schemes, J. Comput. Phys. 126 (1) (1996) 202–228.
[20] N. Kanopoulos, N. Vasanthavada, R.L. Baker, Design of an image edge detection filter using the sobel operator, IEEE J. Solid-State Circuits 23 (2) (1996) 358–367.
[21] M.V. (R2022b), The MathWorks Inc, Natick, Massachusetts, 2022. MATLAB version: 9.13.0
[22] M.H. Center, Documentation. regionprops, Measure properties of image regions, https://www.mathworks.com/help/images/ref/regionprops.html.
[23] C.W. Shu, Essentially non-oscillatory and weighted essentially non-oscillatory schemes for hyperbolic conservation laws, Springer, Berlin Heidelberg; Berlin, Heidelberg, 1998.
[24] D.S. Taubman, M.W. Marcellin, JPEG 2000: Image Compression Fundamentals, Standards and Practice, Norwell, MA, USA, Kluwer Academic Publishers, 2001.
[25] M. Uddin, On the selection of a good value of shape parameter in solving time-dependent partial differential equations using rbf approximation method, Appl. Math. Model. 38 (1) (2014) 135–144.